Max-Planck-Institut für Meteorologie

REPORT No. 92

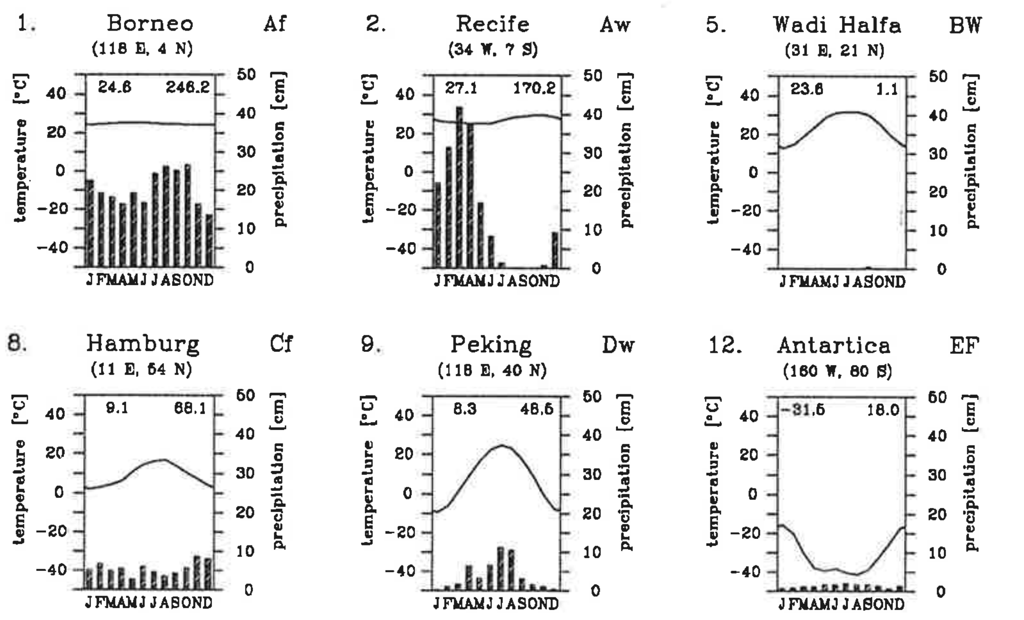

Annual cycles of temperature and precipitation computed from ECHAM3/T42 climatology

THE KÖPPEN CLIMATE CLASSIFICATION AS A DIAGNOSTIC TOOL FOR GENERAL CIRCULATION MODELS

by

ULRIKE LOHMANN • ROBERT SAUSEN • LENNART BENGTSSON
ULRICH CUBASCH • JAN PERLWITZ • ERICH ROECKNER

HAMBURG, OCTOBER 1992

AUTHORS:

Ulrike Lohmann Lennart Bengtsson Erich Roeckner	Max-Planck-Institut für Meteorologie
Robert Sausen Jan Perlwitz	Universität Hamburg Meteorologisches Institut Bundesstraße 55 D-2000 Hamburg 13 FRG
Ulrich Cubasch	Deutsches Klimarechenzentrum (DKRZ) Bundesstraße 55 D-2000 Hamburg 13 FRG
Robert Sausen	Deutsche Forschungsanstalt für Luft- und Raumfahrt (DLR) Institut für Physik der Atmosphäre D-8031 Oberpfaffenhofen FRG

MAX-PLANCK-INSTITUT
FÜR METEOROLOGIE
BUNDESSTRASSE 55
D-2000 HAMBURG 13
F.R. GERMANY

Tel.: +49 (40) 4 11 73-0
Telex: 211092 mpime d
Telemail: MPI.METEOROLOGY
Telefax: +49 (40) 4 11 73-298

REPb 92

ISSN 0937-1060

The Köppen Climate Classification as a Diagnostic Tool for General Circulation Models

Ulrike Lohmann[1], Robert Sausen[2)4], Lennart Bengtsson[1], Ulrich Cubasch[3], Jan Perlwitz[4] and Erich Roeckner[1]

1) Max–Planck–Institut für Meteorologie,
Bundesstraße 55, W–2000 Hamburg 13, Germany

2) Deutsche Forschungsanstalt für Luft– und Raumfahrt (DLR),
Institut für Physik der Atmosphäre,
W–8031 Oberpfaffenhofen, Germany

3) Deutsches Klimarechenzentrum (DKRZ),
Bundesstraße 55, W–2000 Hamburg 13, Germany

4) Meteorologisches Institut der Universität Hamburg,
Bundesstraße 55, W–2000 Hamburg 13, Germany

Abstract

The Köppen climate classification has been applied to the output of atmospheric general circulation models and coupled atmosphere–ocean circulation models. The classification is used for a validation of the control runs of the present climate and for an analysis of greenhouse gas warming simulations. The most prominent results of the global warming computations are the retreat of regions of Permafrost and the increase of areas with Tropical Rainy Climates and Dry Climates.

1 Introduction

For several decades general circulation models of the atmosphere (GCMs) and coupled atmosphere–ocean models have been used for studying climate and climate change. Usually, the models are verified by comparing certain model fields such as the temperature, pressure or wind field with the corresponding analyses. Also higher order quantities such as the low and high frequency variability or the number of blocking events have been studied. The same quantities are usually also analysed in climate change simulations. Besides these direct model variables there are some combinations of variables which comprise usually long time observational knowledge like the classification in Großwetterlagen (Baur, 1963). Another possibility is the classification into climate zones that was introduced by Köppen (1923). Köppen divided the observed climates into several climate zones such as "tropical climate" or "polar climate" by means of the annual cycles of near surface temperature and precipitation. His classification also separates the zones in which different species of plants naturally grow.

Manabe and Holloway (1975) applied the Köppen classification to the model of the Geophysical Fluid Dynamics Laboratory (GFDL). Since that time GCMs have been improved, both in resolution and physical parametrization, and it is worthwhile to apply Köppen's statistics to a state of the art GCM. This method can also be applied to study how climate zones will shift in CO_2 warming experiments.

In Section 2 we will present Köppen's classification and apply it to observations. Then we will use the classification for a validation of the Hamburg atmosphere general circulation model ECHAM3 (Section 3), and we will study the shift of climate zones in greenhouse gas warming simulations performed with the low resolution (T21) coupled atmosphere–ocean model ECHAM1/LSG and performed with the high resolution (T42) atmosphere model ECHAM3 which uses the sea surface temperature change simulated by the coupled model ECHAM1/LSG as input (Section 4). Some concluding remarks (Section 5) will finish the paper.

2 The Köppen Climate Classification

In 1923 Köppen derived an effective classification of climate. Based on the idea that native vegetation is the best expression of climate, Köppen selected climate zone boundaries with the vegetation limits in mind. For instance, the 10°C isoline of the warmest month is connected with the threshold of growing trees. Thus Köppen's classification is based on the direct climate parameters: the annual cycles of temperature and precipitation.

Starting from monthly mean values, we denote the annual mean near surface (2m) temperature by $\bar{t}$, the monthly mean temperature of the warmest and coldest months by t_{max} and t_{min}, respectively. Correspondingly, $\bar{r}$ and r_{min} are the annual mean precipitation and the precipitation of the driest month. Furthermore we define $r_{smax}, r_{smin}, r_{wmax}$ and r_{wmin} as the precipitation of the wettest summer month, the precipitation of the driest summer month, the precipitation of the wettest winter month and the precipitation of the driest winter month, respectively. Here the period from June to August is regarded as northern hemisphere summer and southern hemisphere winter. December to February are the southern hemisphere summer and northern hemisphere winter. For defining the Köppen climate zones (types), temperatures are measured in °C, precipitation in cm/month.

Köppen's classification makes use of a dryness threshold r_d, which depends on the annual mean temperature and the annual cycle of precipitation:

$$r_d \left[\frac{\text{cm}}{\text{month}}\right] = \begin{cases} 2\bar{t}\,[°\text{C}], & \text{if at least 70\% of the annual precipitation occurs in winter;} \\ 2\bar{t}\,[°\text{C}] + 28, & \text{if at least 70\% of the annual precipitation occurs in summer;} \\ 2\bar{t}\,[°\text{C}] + 14, & \text{otherwise.} \end{cases}$$

Köppen distinguished four thermal and one hydrological climate types. Each of the climate types is further differentiated in two or three sub–types. The definition of the climate types and sub–types is given in Table 1. Examples of the different climates types and sub–types will be discussed in Section 3.

We applied the Köppen classification to the temperature data by Jones et al. (1991) and the precipitation data by Legates and Willmott (1990). The Jones data are monthly mean values of the sea level temperature averaged over the period 1951–1980. For our purposes we determined the near surface temperature using the mean orography and assuming a lapse rate of 0.65 K / 100 m. The precipitation data are based on observations from 1920 to 1980. However, data from recent years got a higher weight in the averaging procedure. Precipitation over the oceans was interpolated from coastal and island stations. Systematic errors were removed by regression analyses. South of 30°S Legates and Willmott (1990) used the Jaeger (1976) data. The spatial resolution of data is reduced to the Gaussian grid used in a T21 spectral model (approx. 5.6°).

Figure 1 (upper panel) shows the climate zones determined from the data by Jones and Legates, hereafter referred as J+L. Köppen's chart (Figure 2) is well reproduced apart from the Dry Climates (B), which extend far north of the Himalaya in Köppen's chart. The

Table 1: Climate classification after Köppen

Type	Sub–type	Name	Criterion
A		**Tropical Rainy Climates**	$t_{min} \geq 18°C$
	Af	Tropical Rainforest Climate	$r_{min} \geq 6 \frac{cm}{month}$
	Aw	Tropical Savanna Climate	$r_{min} < 6 \frac{cm}{month}$
B		**Dry Climates**	$\overline{r} \geq r_d$
	BS	Steppe Climate	$\overline{r} \geq \frac{r_d}{2}$
	BW	Desert Climate	$\overline{r} < \frac{r_d}{2}$
C		**Humid Mesothermal Climates**	$-3°C \leq t_{min} < +18°C$
	Cs	Warm Climate with Dry Summer	$r_{wmax} \geq 3 \cdot r_{smin}$
	Cw	Warm Climate with Dry Winter	$r_{smax} \geq 10 \cdot r_{wmin}$
	Cf	Humid Temperate Climate	$r_{smax} < 10 \cdot r_{wmin}$ and $r_{wmax} < 3 \cdot r_{smin}$
D		**Humid Microthermal Climates**	$t_{min} < 3°C$ and $t_{max} \geq 10°C$
	Dw	Cold Climate with Dry Winter	$r_{smax} \geq 10 \cdot r_{wmin}$
	Df	Cold Climate with Moist Winter	$r_{smax} < 10 \cdot r_{wmin}$
E		**Polar Climates**	$t_{max} < 10°C$
	ET	Tundra Climate	$0°C \leq t_{max} < +10°C$
	EF	Permafrost Climate	$t_{max} < 0°C$

weak correspondence over the oceans concerning the Dry Climates (B) and the distribution of Humid Mesothermal Climates (C) is quite different in both charts and may be due to the lack of observations.

For illustration, also the Jaeger (1976) precipitation data have been used directly to produce a climate zone chart (Figure 1, lower panel), hereafter cited as J+J. Figure 3 (upper panel) shows the fraction of the globe and of the continents, covered by the different climate types and sub–types (see also Tables A1 and A2 in the appendix). Compared to J+L, the Dry Climates (BW, BS) in J+J cover larger areas, especially over oceans, whereas less Tropical Savanna (Aw) is found in J+J. Another major difference is detected in regions, where J+J shows a Humid Temperate Climate (Cf) while J+L has a Mediterranean Climate (Cs), e.g. over the North Atlantic Ocean and the North Pacific Ocean. The differences of the two classifications resulting mainly from different precipitation data indicate the uncertainties of the observations that should be kept in mind when evaluating model climates.

3 Simulation of the Climate Zones with the Atmosphere Model ECHAM3

Based on the numerical weather prediction model of ECMWF[1], the spectral general circulation model ECHAM has been developed jointly by the Meteorologisches Institut der Universität Hamburg and the Max–Planck–Institut für Meteorologie, Hamburg. Prognostic variables are vorticity, divergence, temperature, (logarithm of) surface pressure, humidity and cloud liquid water (ice and water phase). The model contains parametrizations of radiation, cloud formation and precipitation, convection, and vertical and horizontal diffusion. Land surface processes are described by a five layer heat conductivity soil model and by a hydrological model to determine evaporation and runoff. The model is currently used in two different horizontal resolutions mainly: T21 and T42. The corresponding Gaussian grids for calculating the non–linear and the diabatic terms have a resolution of approx. 5.6° and 2.8°, respectively. The model uses 19 vertical layers in a hybrid σ–p–coordinate system. The annual and daily cycles of the solar radiation are included. The annual cycle of the sea surface temperature is prescribed. Currently three version of the model exist (ECHAM1, ECHAM2, ECHAM3), representing successively more advanced versions. A comprehensive description can be found in Roeckner et al. (1992), which also contains a basic climatology of the model.

Here we will study two long term integrations performed with ECHAM3 at T21 and T42 resolution, respectively. For both runs the climatological sea surface temperature was prescribed (based on the observations of the years 1979–88). Figure 4 (lower panel) shows the climate zones as simulated at the T21 resolution. The basic features of the observations (Figure 1) are reproduced, apart from the Dry Climates (B). They cover 17.6% in the simulation, whereas only 9.9% of the globe is classified by J+L (14.6% by J+J, see also Figure 3). No Dry Climates (B) show up North of the Himalaya (for example Gobi Desert). The Sahara Desert and the Arabian Desert extend too far north. In contrast to the observations the model simulates Permafrost (EF) for the whole Arctic Ocean (except of the region north of Scandinavia and Russia). However, this is an artefact of the model as sea ice of 2 m thickness without leads is prescribed all over the year.

The shift of climate zones can be made more obvious, if the transfer matrices are considered (Table 2). The left panel takes the whole surface of the globe into account, the right panel only land points. The numbers give the percentage of area that is of type X in J+L, but of type Y in ECHAM3/T21, e.g. 4.9% of the area is of type A in J+L, but of type B in ECHAM3/T21. If the climates were identical in both realisations, numbers would

[1]ECMWF = European Center for Medium Range Weather Forecasts

Table 2: Transfer matrices from observations (J+L) to the uncoupled reference simulation with ECHAM3/T21 (S21). The numbers denote the percentage of the globe which is of type i in J+L but of type j in S21. Only values equal or larger 0.1 are listed. Left: land and ocean, right: only continental points. The numbers in the upper left corner are the sum of the matrix elements in the main diagonal (d), above (a) and below (b) the main diagonal, respectively.

d=86.5		S21				
a=6.8 b=6.7		A	B	C	D	E
J+L	A	30.6	4.9	0.2		
	B	0.7	8.9	0.3	0.1	
	C	1.0	3.5	27.7	0.1	0.4
	D		0.3	0.4	6.1	0.9
	E			0.6	0.1	13.3

d=86.4		S21				
a=4.7 b=8.9		A	B	C	D	E
J+L	A	20.3	0.8	0.7		
	B	1.0	13.4	1.0	0.2	
	C	1.5	3.8	14.0	0.2	
	D		1.2	0.7	19.7	1.8
	E			0.2	0.3	19.0

occur only on the main diagonal. If the sum of the numbers above the main diagonal is larger than the sum of the numbers below, the second realisation has a colder climate.

With regard to the large scale pattern, the T42 simulation with ECHAM3 (Figure 5, upper panel) is quite similar to the T21 reference simulation, but resolves more regional features. Examples of such features are the desert areas (BW) north of the Himalaya and the Tropical Rain Forest (Af) in Central Africa. But also some model biases show up, like the desert which extends too far south in East Africa, or the Cs climate in Western Europe, where Köppen (1923) shows Cf climate. However, such features are already beyond the dynamical resolution of the model (approx. 480 km). Apart from such very small scale features, the Köppen chart (1923) is reproduced reasonably well.

As the Gaussian grids corresponding to the spectral resolutions of T21 and T42 do not coincide, we do not calculate the transfer matrices from observed climates or T21 model climates to the T42 model climate. Nevertheless we can compare the fraction of the globe (continents) covered by a certain climate type or sub–type (Figure 3, upper panel). Obviously, the T42 simulation shows the largest fraction of B climates, in particular BW. On the other hand, C and D climates are underestimated.

To illustrate the Köppen climate zones further, Figure 6 shows the annual cycles of temperature and precipitation at selected grid points (simulated by ECHAM3/T42). The geographic position of the points is indicated by numbers in Figure 7. The indicated geographical longitudes and latitudes refer to the centre of the grid cell. The name refers to a place located in the grid cell. Two grid boxes with steppe climate (BS) were selected, one representing a warm subtropical steppe (No 3, Zinder (Niger)) and one representing a cold mid–latitude steppe (No 4, Karaganda (Kazakhstan)).

4 Shifting of Climate Zones in Greenhouse Gas Warming Simulations

In recent years the impact of the anthropogenic change in the greenhouse gas concentration has been studied with a variety of coupled atmosphere–ocean models. Cubasch et al. (1992) performed a series of four 100 year simulations with the coupled atmosphere–ocean model ECHAM1/LSG. The atmospheric component of this coupled model (at T21 horizontal resolution) differs from ECHAM3/T21, which has been described in Section 3, with respect to several aspects of the physical parameterizations. As is described in Roeckner et al. (1992), the ECHAM1 used, for example, the so called Kuo convection scheme as well as an overly enhanced orographic forcing including both the envelope orography and gravity wave drag.

The ocean model LSG is based on a numerical formulation of the primitive equations (Maier–Reimer and Hasselmann, 1987; Mikolajewicz and Maier–Reimer, 1990) appropriate for Large Scale Geostrophic motion. The non–linear advection of momentum is negleted and fast gravity waves are strongly damped by an implicit time integration scheme using a time step of 30 days. The salinity and temperature transports through currents are computed with an up–stream advection scheme. Vertical convective mixing is applied whenever the stratification becomes unstable. Sea–ice is computed from the ice heat balance and the advection by ocean currents, using a simplified viscous rheology. A realistic bottom topography is included.

The discretisation of the ocean model is based on 11 variably spaced vertical levels and two overlapping $5.6° \times 5.6°$ horizontal E–grids (resulting in an effective grid–size of 4°), which corresponds to the T21 Gaussian grid of ECHAM. In the coupled model simulations, the basic timestep of 30 days is reduced to 1 day for the computation of the sea–ice and the temperature and salinity in the two uppermost ocean levels in order to resolve the more rapid response of the upper ocean to the short–term variability of the atmosphere.

The atmosphere and ocean components are coupled by the air–sea fluxes of momentum, energy (sensible and latent heat, shortwave and longwave radiation) and fresh water (precipitation minus evaporation plus river runoff along the coastal boundaries). The fluxes are calculated in ECHAM, using the sea surface temperature and sea–ice thickness from LSG as surface boundary conditions. To avoid a climate drift of the coupled system, a flux correction is applied (Sausen et al., 1988). Both models were integrated synchroneously, but with their different time steps.

Four different CO_2 scenario simulations were conducted extending over 100 model years,

Table 3: As Table 2, but for the T21 uncoupled reference simulation with ECHAM3 (S21) and the T21 coupled control simulation with ECHAM1/LSG (CTL).

d=85.4		CTL				
a=6.9 b=7.7		A	B	C	D	E
S21	A	29.4	1.3	1.6		
	B	3.9	10.8	2.5	0.4	
	C		0.3	27.9	0.9	0.0
	D		0.2	0.1	5.9	0.1
	E			1.4	1.7	11.5

d=78.4		CTL				
a=14.3 b=7.3		A	B	C	D	E
S21	A	15.3	4.2	3.4		
	B	0.8	14.8	2.3	1.3	
	C		0.7	13.3	2.7	
	D		0.7		19.3	0.4
	E				5.1	15.7

respectively: Control ("1×CO_2"), instantaneous doubling of CO_2 ("2×CO_2"), IPCC Scenarios A and D (Houghton et al., 1990). In the control run the global mean of the sea surface temperature was quite stationary, showing a decrease of less than 0.4 K during the 100 year integration. In the "2×CO_2" experiment the temperature increased by 1.7 K in 100 years. For Scenarios A and D the temperature rises are 2.6 K and 0.6 K, respectively. More details of the experiments and their results can be found in Cubasch et al. (1992).

In the current paper we will concentrate on the Köppen climate zones simulated in the last decade of the Control and the Scenario A experiments. Figure 3 (lower panel) shows the fraction of area of the globe (continents) covered by the individual climate types and sub-types. In Figure 8 (upper panel) the Köppen climate zones for the control experiment (mean of the years 91 to 100) are plotted. The main features of the (quite realistic) ECHAM3/T21 uncoupled reference simulation (Figure 4, lower panel) are reproduced. A more detailed analysis, however, shows that the warmer climates are less often simulated, in particular Aw and BW (see also Tables A1 and A2 in the Appendix). This becomes more obvious if the transfer matrices are considered (Table 3).

However, this shift in climate zones can only partly be attributed to a climate drift due to the coupling of the ocean and atmosphere models. The atmospheric component of the coupled model used an earlier version of ECHAM than that discussed in Section 3. Thus, the coupled control integration should rather be compared with an uncoupled run performed with ECHAM1/T21. Also with this version a 20 year reference integration was performed (20 identical cycles of sea surface temperature). Figure 4 (upper panel) shows the Köppen climate zones for this run. Obviously the differences due to the coupling are weaker. This is assured by the transfer matrices (Table 4, see also Tables A1 and A2 in the appendix). A bias like the desert in the Amazon basin, which is also found in the ECHAM1 reference simulation, can be attributed to the severe truncation enhanced by the use of an envelope orgraphy in ECHAM1 (caused by the Gibbs phenomenon).

Table 4: As Table 2, but for the T21 uncoupled reference simulation with ECHAM1 (EC1) and the T21 coupled control simulation with ECHAM1/LSG (CTL).

d=94.6		CTL				
a=3.6 b=1.8		A	B	C	D	E
	A	32.5	0.1	1.9		
	B	0.8	12.5	0.8	0.2	
EC1	C		0.1	30.1	0.4	0.1
	D		0.1		8.2	0.2
	E			0.7	0.2	11.3

d=92.5		CTL				
a=6.8 b=0.7		A	B	C	D	E
	A	15.8	0.3	2.8		
	B	0.3	19.9	1.4	0.6	
EC1	C			14.7	1.0	
	D		0.2		26.6	0.7
	E				0.2	15.5

Table 5: As Table 2, but for the T21 coupled control simulation and the T21 coupled ECHAM1/LSG (CTL) with Scenario A (SCA).

d=89.7		SCA				
a=0.9 b=9.4		A	B	C	D	E
	A	32.4	0.9			
	B	0.2	12.5			
CTL	C	4.1	1.1	28.2		
	D		0.3	1.6	7.0	
	E			1.2	0.8	9.6

d=83.8		SCA				
a=1.6 b=14.6		A	B	C	D	E
	A	14.5	1.5			
	B	0.3	20.1			
CTL	C	5.1	1.6	12.2		
	D		1.2	4.4	22.8	
	E				2.1	14.1

The Scenario A global warming experiment is analysed in Figure 8 (lower panel). The most prominent feature is a reduction of the Permafrost area (EF, from 7.0% to 5.1%). The Arctic Sea is free of ice. Consistent to the dislocation of sea–ice, Tundra Climate (ET) in Northern Siberia is replaced by Cold Climate with Moist Winter (Df). Another substantial change in climate is the increase of the Tropical Rainy Climates (Af, from 33.3% to 36.7%), which can be seen in equatorial Africa or in South America. Also the Dry climates (B) cover larger areas, they increase from 20.4% to 24.5% of the continental areas (see also Figure 3). Figure 9 localizes the grid points with a shift towards a colder climate (downward in Table 1) and to warmer climate (upward in Table 1). Climate sub–types are not regarded. In 9.4% and 0.9% of the grid points the Scenario A climate is of a warmer and colder type, respectively (see also Table 5).

Finally, we examined a Scenario A experiment (A42) performed with the uncoupled ECHAM3 at T42 horizontal resolution (Perlwitz, 1992). As a 100 year simulation with ECHAM3/T42 would require more computational resources than presently available, the technique of time slicing was applied: First, the difference of the sea surface temperatures between Scenario A (mean of years 91–100)and the control integration (mean of years 1–10) was determined from the simulations with the coupled model ECHAM1/LSG. This difference was then added to the climatological sea surface temperature (same as used for the ECHAM3/T42 reference simulation (S42) mentioned in Section 3). Using the modified sea surface temperature, a 10 year integration was performed with the uncoupled atmosphere model ECHAM3/T42. This is a kind of a stationary Scenario A experiment. The global mean sea surface temperature is 2.0 K higher on average then in the reference simulation (S42).

This Scenario A simulation (A42) allows to study the change of the climate zones in more detail. Figure 5 shows the Köppens climate zones both for the reference simulation (upper panel) and for Scenario A (lower panel). As in the case of the T21 coupled ECHAM1/LSG simulations, the retreat of the Permafrost Climate (EF) is obvious, we find a reduction from 7.2% to 5.2% (see also Figure 3 and Tables in the Appendix). Again an increase of the Tropical Savanna Climate (Aw) is observed (from 22.5% to 23.9%), but the change is less pronounced than in the coupled simulations (CTL vers. SCA). The Dry Climates (B), in particular the Desert Climate (BW) cover a larger area. The Humid Mesothermal Climates (C) show a reduction in general. In Eastern Europe it drives away the Humid Microthermal Climate (D), altough the D Climates cover a larger area (e.g. in North–East Siberia). The general shift towards warmer climates is also obvious from Table 6. Finally, Figure 10 shows where the changes of climate types can be observed. In 13.8% of the continents the Scenario A (A42) climate is of a warmer type and only in 0.9% of a colder type.

In the IPCC report, Mitchell et al. (1990) selected five different climatic areas, where they estimated the regional changes of temperature, precipitation and soil wetness in the year 2030 according to the "business as usual" scenario from a simplified model, which is identical to the Scenario A used in our experiment. In each of these areas the temperature rises (from 1 to 4 K), but the precipitation changes in both directions. In Central North America they estimate a warming of 2–4 K and increased precipitation of 0–15% in winter, whereas the precipitation decreases in summer by 5–10%. Going along with this, ECHAM3/T42 Scenario A shows more Humid Temperate Climate (Cf) instead of Cold Climate with Moist Winter (Df) in this region. In Southern Asia, A42 simulates Savanna (Aw) that replaces Warm Climate with Dry Winter (Cw). This is consistent with the increased summer precipitation (5–15%) and higher temperature (1–2 K) in Mitchell et al.. The Dry Climates (B) extend far south of the Sahara in Scenario A, whereas in Mitchell et al. temperature (1–2 K) and area mean precipitation in the Sahel zone rise. Since the Dry Climates are dependent on temperature and precipitation, a warmer climate with little increased precipitation could nevertheless be a Dry Climate. For Southern Europe Mitchell et al. compute a warming by 2 K and an increased precipitation in

Table 6: As Table 2, but for the uncoupled T42 ECHAM3 simulation for the reference case (S42) and for the Scenario A case (A42).

d=89.5		A42				
a=2.1 b=8.4		A	B	C	D	E
	A	31.2	1.9			
	B	0.4	18.8	0.1		
S42	C	2.8	1.3	24.2		0.1
	D		0.2	0.8	4.9	
	E			1.2	1.5	10.4

d=85.3		A42				
a=0.9 b=13.8		A	B	C	D	E
	A	22.2	0.7			
	B	0.2	22.4	0.3		
S42	C	3.5	1.5	10.8		
	D		0.9	2.8	15.7	
	E			0.1	4.8	14.1

winter. During summer the temperature is also higher (2–3 K), but the precipitation is reduced by 5–15%. Corresponding to this, ECHAM3/T42 shows a shift from Warm Humid Climate (Cf) to Warm Climate with Dry Summer (Cs) in Central Europe and an expansion of Steppe (BS) far North in South–West Europe. In Australia ECHAM3/T42 predicts extended Savanna regions (Aw) consistent with an increase in temperature by 1–2 K and precipitation by 10% as forecast by Mitchell et al..

5 Concluding remarks

We applied the Köppen climate classification to a series of uncoupled and coupled simulations with the atmosphere general circulation model ECHAM. The uncoupled model ECHAM, especially the versions ECHAM2 (not shown) and ECHAM3, reproduces the observations rather well. Even small scale features like the Gobi desert, for example, are reproduced in the ECHAM3/T42 reference simulation.

The control climate of the coupled model ECHAM1/LSG (T21) is somewhat too cold, especially in the tropics, relative to the uncoupled reference climate. The greenhouse gas warming computations with this model exhibit a retreat of the Permafrost Climate and a progression of both the Tropical Rainy Climates and the Dry Climates. This result remains true for the uncoupled ECHAM3/T42 simulations. The result for the Humid Microthermal Climates is of opposite sign in both the coupled T21 and uncoupled T42 simulations, indicating the uncertainty of the model results.

An extension of the Köppen climate zones is the calculation of (stationary) biomes (Claussen and Esch, 1992), which considers more model data relevant for biological systems. However, the Köppen classification is easier to apply and is still a useful tool to estimate the skill of climate models in reproducing the present climate as well as indicating the impact of climate changes on the biosphere.

Appendix

Table A1: Fraction of the globe covered by the different climate zones [%] for observations and model simulations.

Climate zone	J+J	J+L	EC1	S21	S42	CTL	SCA	A42
A	31.8	35.6	34.5	32.3	33.1	33.3	36.7	34.4
Af	14.9	14.0	13.2	9.5	10.6	13.6	14.8	10.5
Aw	16.9	21.6	21.3	22.8	22.5	19.7	21.9	23.9
B	14.6	9.9	14.3	17.6	19.4	12.7	14.8	22.3
BS	7.3	5.4	6.3	5.9	6.6	6.2	6.7	7.8
BW	7.3	4.5	8.0	11.7	12.8	6.5	8.1	14.5
C	31.9	32.8	30.7	29.1	28.5	33.5	31.1	26.3
Cs	2.6	7.2	9.4	8.6	11.0	9.1	9.9	10.3
Cf	26.8	21.0	19.8	18.1	15.3	21.9	20.0	14.8
Cw	2.5	4.6	1.5	2.4	2.2	2.5	1.2	1.2
D	7.8	7.8	8.5	6.3	6.0	8.9	7.8	6.4
Df	6.6	6.5	7.9	6.0	5.5	8.5	7.3	6.1
Dw	1.2	1.3	0.6	0.3	0.5	0.4	0.5	0.3
E	13.9	13.9	12.2	14.6	13.1	11.6	9.6	10.5
ET	8.4	8.4	5.4	6.8	5.9	4.6	4.5	5.3
EF	5.5	5.5	6.8	7.8	7.2	7.0	5.1	5.2

J+J: Observations based on Jones et al. (1991) and Jaeger (1976);
J+L: Observations based on Jones et al. (1991) and Legates and Willmott (1990);
EC1: T21 uncoupled reference simulation with ECHAM1;
S21: T21 uncoupled reference simulation with ECHAM3;
S42: T42 uncoupled reference simulation with ECHAM3;
CTL: T21 coupled control simulation with ECHAM1/LSG;
SCA: T21 coupled Scenario A simulation with ECHAM1/LSG;
A42: T42 uncoupled Scenario A simulation with ECHAM3.

Table A2: As Table A1, but only for continental areas.

Climate zone	J+J	J+L	EC1	S21	S42	CTL	SCA	A42
A	22.6	21.8	18.9	22.8	22.9	16.1	19.9	26.0
Af	3.2	4.5	2.4	1.6	2.7	2.6	3.1	3.2
Aw	19.4	17.3	16.5	21.2	20.2	13.5	16.8	22.8
B	15.1	15.6	22.2	19.6	23.0	20.4	24.5	25.4
BS	5.7	6.4	7.8	4.1	7.0	7.4	9.0	8.5
BW	9.4	9.2	14.4	15.5	16.0	13.0	15.5	16.9
C	19.1	19.5	15.7	16.6	15.8	18.9	16.7	14.9
Cs	2.3	3.0	4.7	2.7	2.5	4.5	7.5	4.1
Cf	11.1	10.9	6.1	5.6	5.4	6.0	5.3	5.5
Cw	5.7	5.6	4.9	8.3	7.9	8.4	3.9	4.3
D	23.7	23.5	27.5	20.1	19.4	28.4	24.8	20.6
Df	19.4	19.0	25.5	19.1	17.7	26.9	23.2	19.4
Dw	4.3	4.5	2.0	1.0	1.7	1.5	1.6	1.2
E	19.6	19.6	15.7	20.8	19.0	16.2	14.1	14.2
ET	9.6	9.6	5.7	9.7	7.9	5.8	4.3	3.5
EF	10.0	10.0	10.0	11.1	11.1	10.4	9.8	10.7

Acknowledgement. This study was supported by the Bundesminister für Forschung und Technologie (BMFT), grant 07 KFT 05/6. We also would like to thank Jörg Kaduk and Martin Heimann for providing us the coloured graphics routines.

References

Baur, F., 1936: Wetter, Witterung, Großwetter and Weltwetter. *Z. angew. Met. 56*, 377–381.

Claussen, M. and M. Esch, 1992: Biomes computed from simulated climatologies. *Report No. 89, Max–Planck–Institut für Meteorologie.*, 19pp.

Cubasch, U., K. Hasselmann, H. Höck, E. Maier–Reimer, U. Mikolajewicz, B. D. Santer and R. Sausen, 1991: Time–dependent greenhouse warming computations with a coupled ocean–atmosphere model. Climate Dyn., in press.

Houghton J. T., G. J. Jenkins and J. J. Ephraums, 1990: Climate Change. The IPCC Scientific Assessment. Cambridge University Press, Cambridge, 365 pp.

Jaeger, L., 1976: Monatskarten des Niederschlags für die ganze Erde. Berichte des Deutschen Wetterdienstes, Offenbach a.M., *139*, 38 pp.

JONES, P. D., T. M.L. WIGLEY, G. FARMER, 1991: Marine and land temperature data sets: A comparison and a look at recent trends. In M. E. Schlesinger (ed.): Greenhouse–Gas–Induced Climatic Change: A Critical Appraisal of Simulations and Observations, *19*, Elsevier, Amsterdam, 153–172.

KÖPPEN, W., 1923: Die Klimate der Erde. Walter de Gruyter, Berlin, 369 pp.

LEGATES, D. R. AND C. J. WILLMOTT, 1990: Mean Seasonal and Spatial Variability in Gauge–Corrected, Global Precipitation. *Int. J. Climatol.* *10*, 111–127.

MAIER–REIMER, E. AND K. HASSELMANN, 1987: Transport and storage of CO_2 in the ocean–an inorganic ocean–circulation carbon cycle model. *Climate Dyn.* *2*, 63–90.

MIKOLAJEWICZ, U. AND E. MAIER–REIMER, 1990: Internal secular variability in an ocean general circulation model. *Climate Dyn.* *4*, 145–156.

MANABE, S., J. L. HOLLOWAY, 1975: The Seasonal Variation of the Hydrologic Cycle as Simulated by a Global Model of the Atmosphere. *J. Geophys. Res.* *80*, 1617–1649.

MITCHELL, J. F. B., S. MANABE,T. TOKIOKA AND V. MELESHKO, 1990: Equilibrium climate change and its implications in the future. In Houghton J. T., G. J. Jenkins and J. J. Ephraums: Climate Change. The IPCC Scientific Assessment. Cambridge University Press, Cambridge, 131-172.

PERLWITZ, J., 1992: Preliminary results of a global SST anomaly experiment with a T42 GCM. *Ann. Geophys.* Supplement II to Vol. 10, C296.

ROECKNER, E., K. ARPE, L. BENGTSSON, S. BRINKOP, L. DÜMENIL, M. ESCH, E. KIRK, F. LUNKEIT, M. PONATER, B. ROCKEL, R. SAUSEN, U. SCHLESE, S. SCHUBERT AND M. WINDELBAND, 1992: Simulation of the present–day climate with the ECHAM model: Impact of model physics and resolution.*Report No. 95, Max–Planck–Institut für Meteorologie*, in press.

SAUSEN, R. , K. BARTHEL AND K. HASSELMANN, 1988: Coupled ocean–atmosphere models with flux correction. *Climate Dyn.* *2*, 154–163.

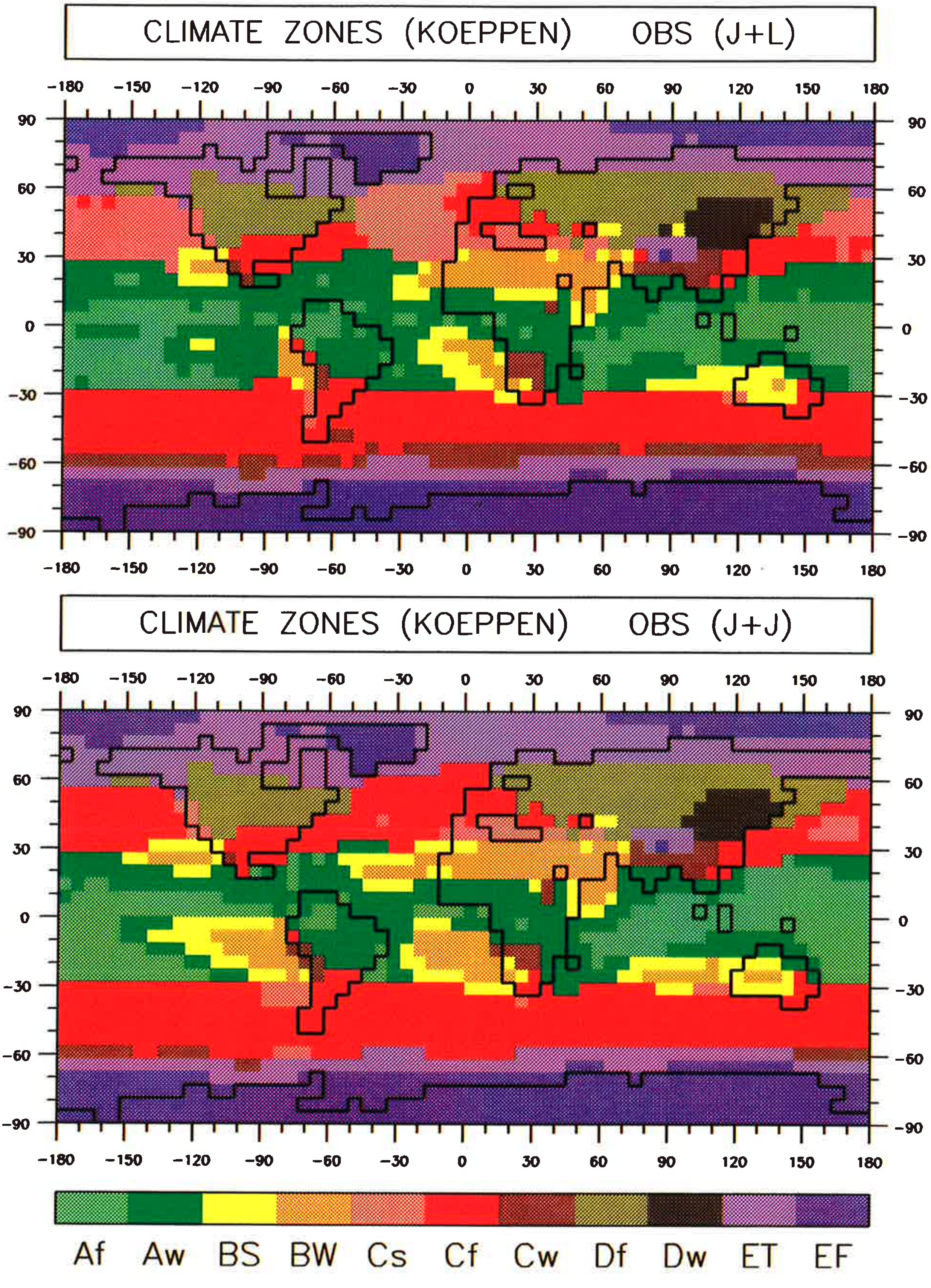

Figure 1: Observed climate zones.
Top: based on the Jones et al. (1991) and the Legates and Willmott (1990) data.
Bottom: based on the Jones et al. (1991) and the Jaeger (1976) data.

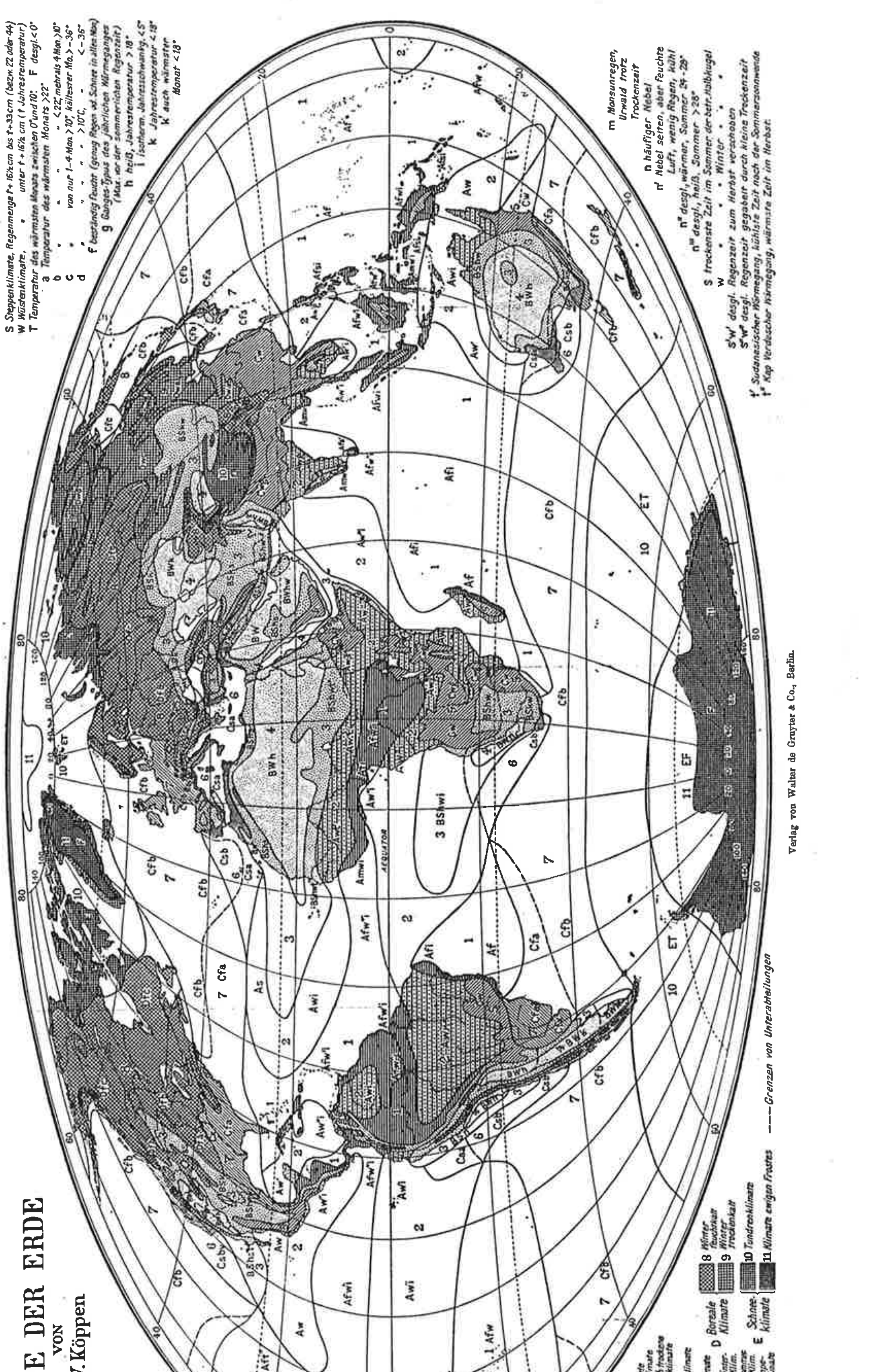

Figure 2: Reproduction of Köppen's chart of climate zones (after Köppen, 1923)

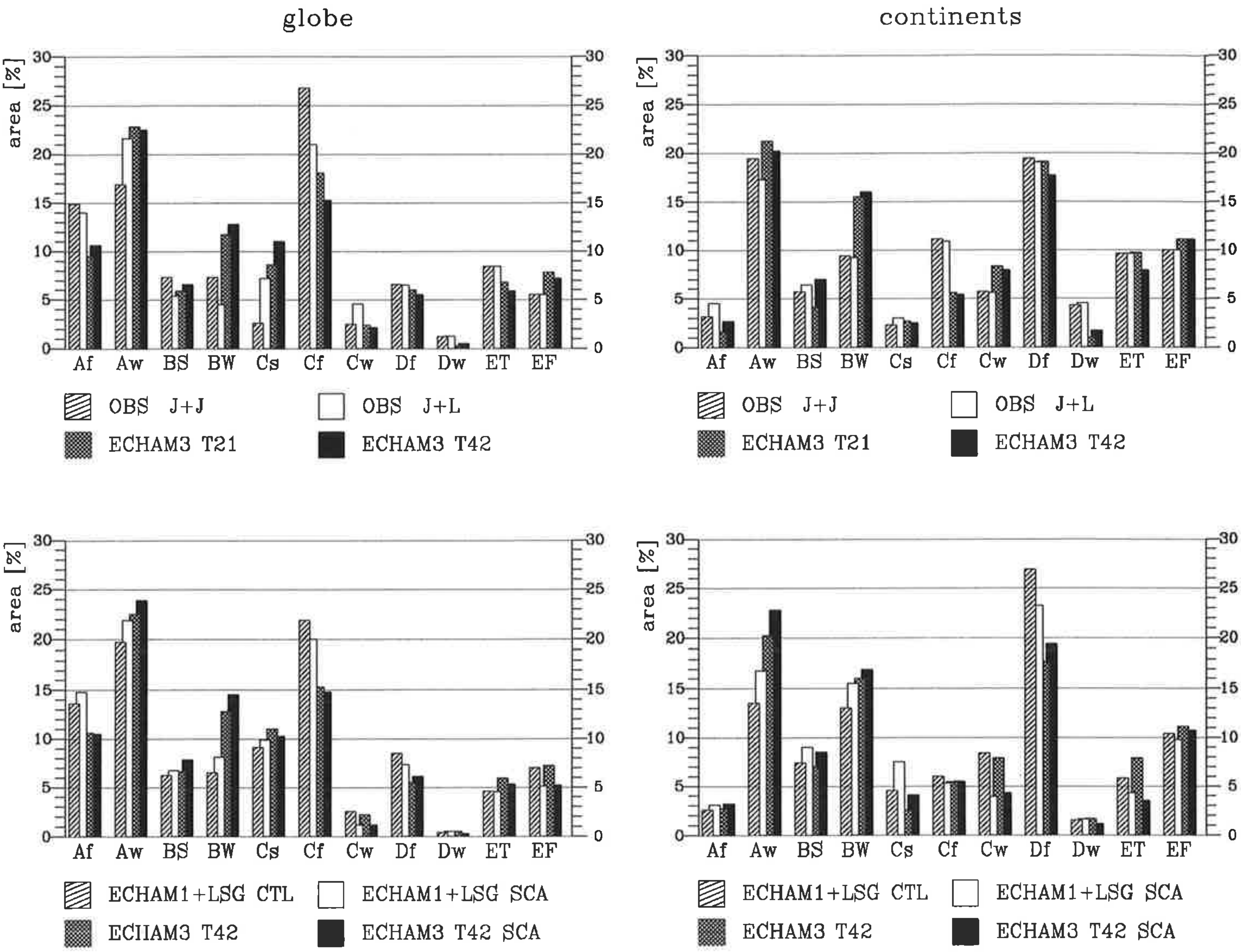

Figure 3: Fraction of the globe (left panel) and of the continents (right panel) covered by different climate zones for observations and model simulations.
Upper panel:
J+J: Observations based on Jones et al. (1991) and Jaeger et al. (1976);
J+L: Observations based on Jones et al. (1991) and Legates and Willmott (1990);
S21: T21 uncoupled reference simulation with ECHAM3;
S42: T42 uncoupled reference simulation with ECHAM3.
Lower panel:
CTL: T21 coupled control simulation with ECHAM1/LSG;
SCA: T21 coupled Scenario A simulation with ECHAM1/LSG;
S42: T42 uncoupled reference simulation with ECHAM3;
A42: T42 uncoupled Scenario A simulation with ECHAM3.

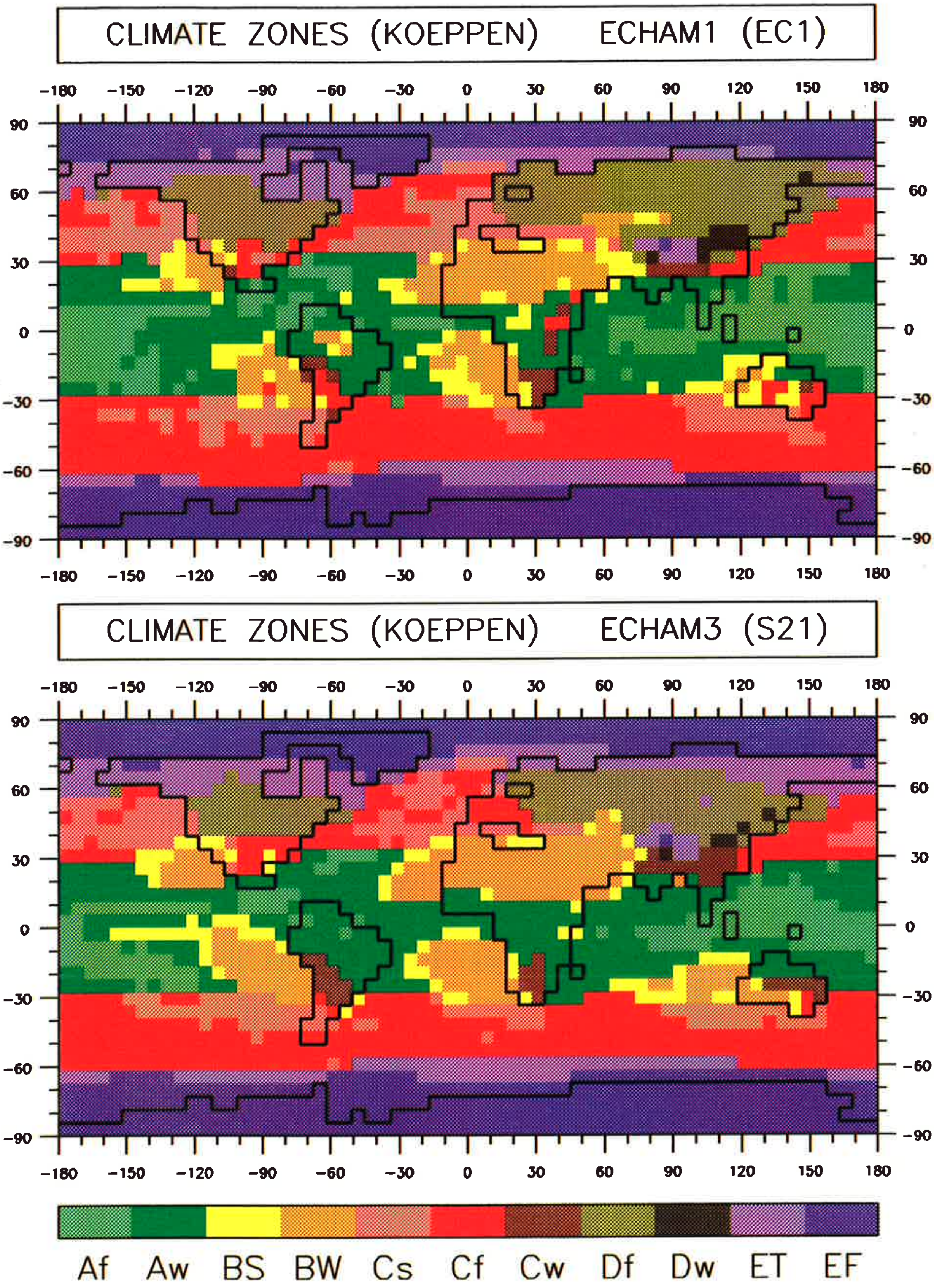

Figure 4: Köppen climate zones as simulated by ECHAM1/T21 (upper panel) and by ECHAM3/T21 (lower panel) in reference runs with climatological sea surface temperature.

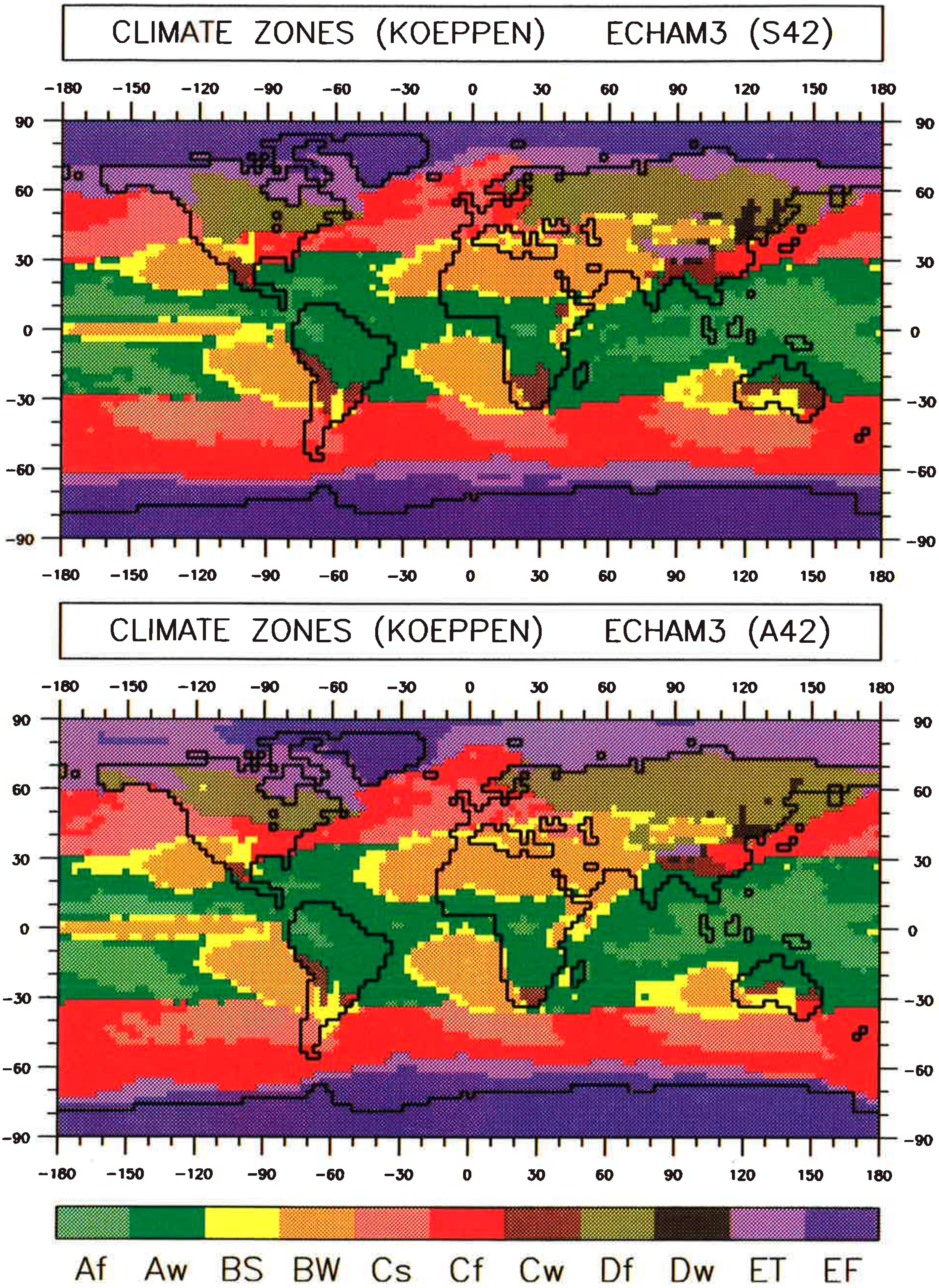

Figure 5: Köppen climate zones as simulated by ECHAM3 (T42 horizontal resolution) in a reference run (upper panel) and in a Scenario A simulation (lower panel).

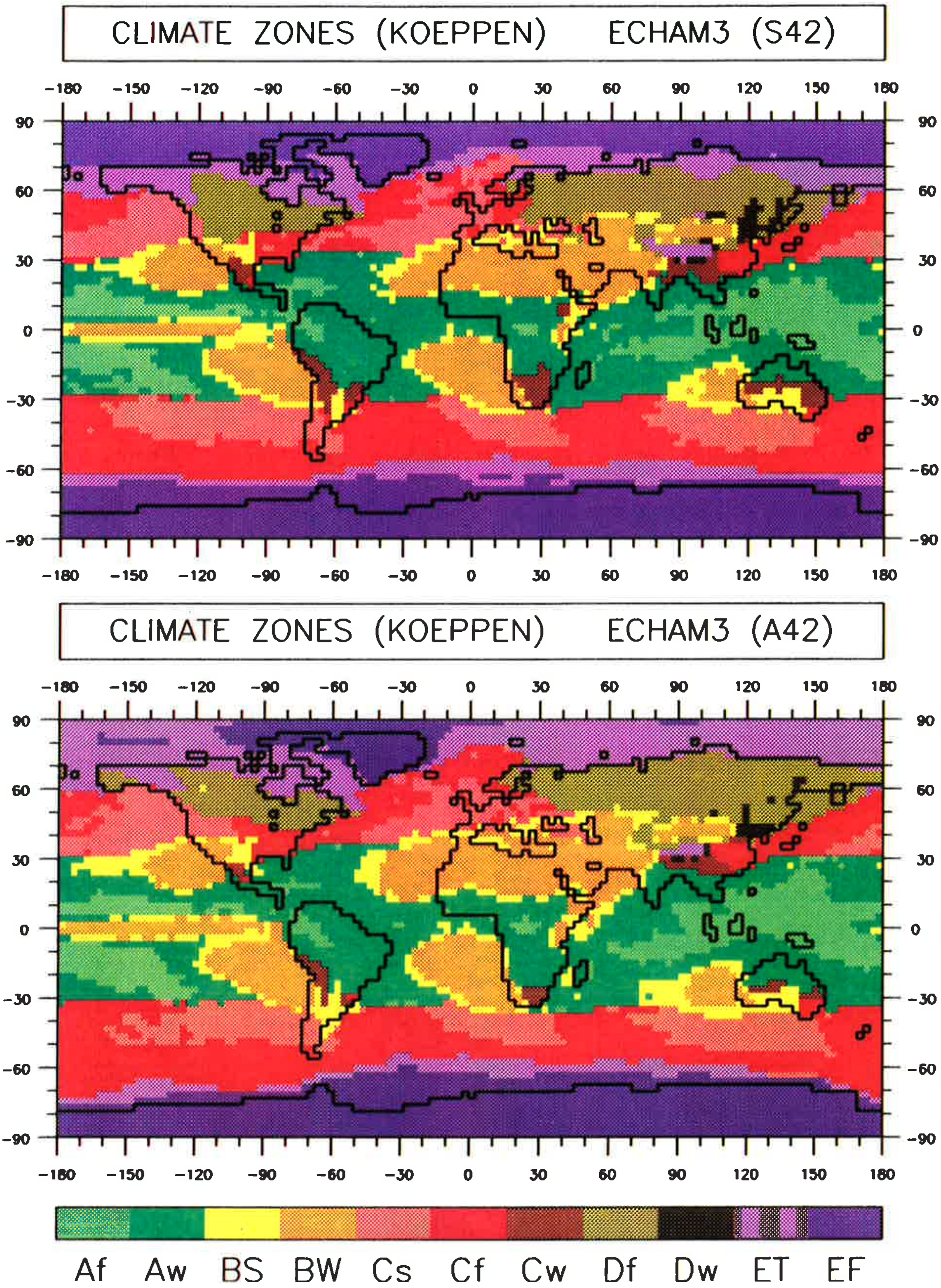

Figure 5: Köppen climate zones as simulated by ECHAM3 (T42 horizontal resolution) in a reference run (upper panel) and in a Scenario A simulation (lower panel).

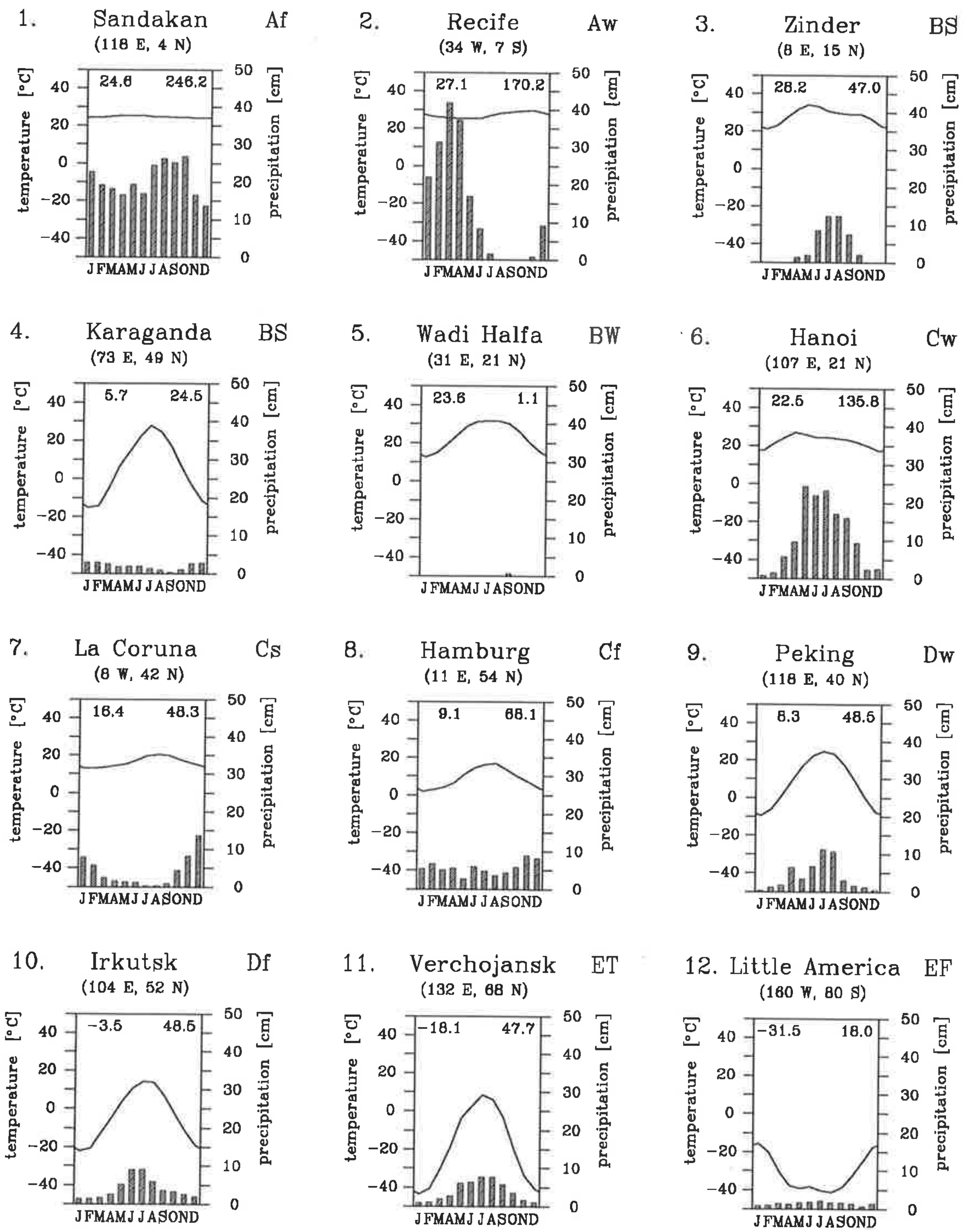

Figure 6: Annual cycles of temperature and precipitation at selected grid points representing the different Köppen climate sub–types (from the T42 reference simulation with ECHAM3). The geographical positions of the points are indicated in Figure 7.

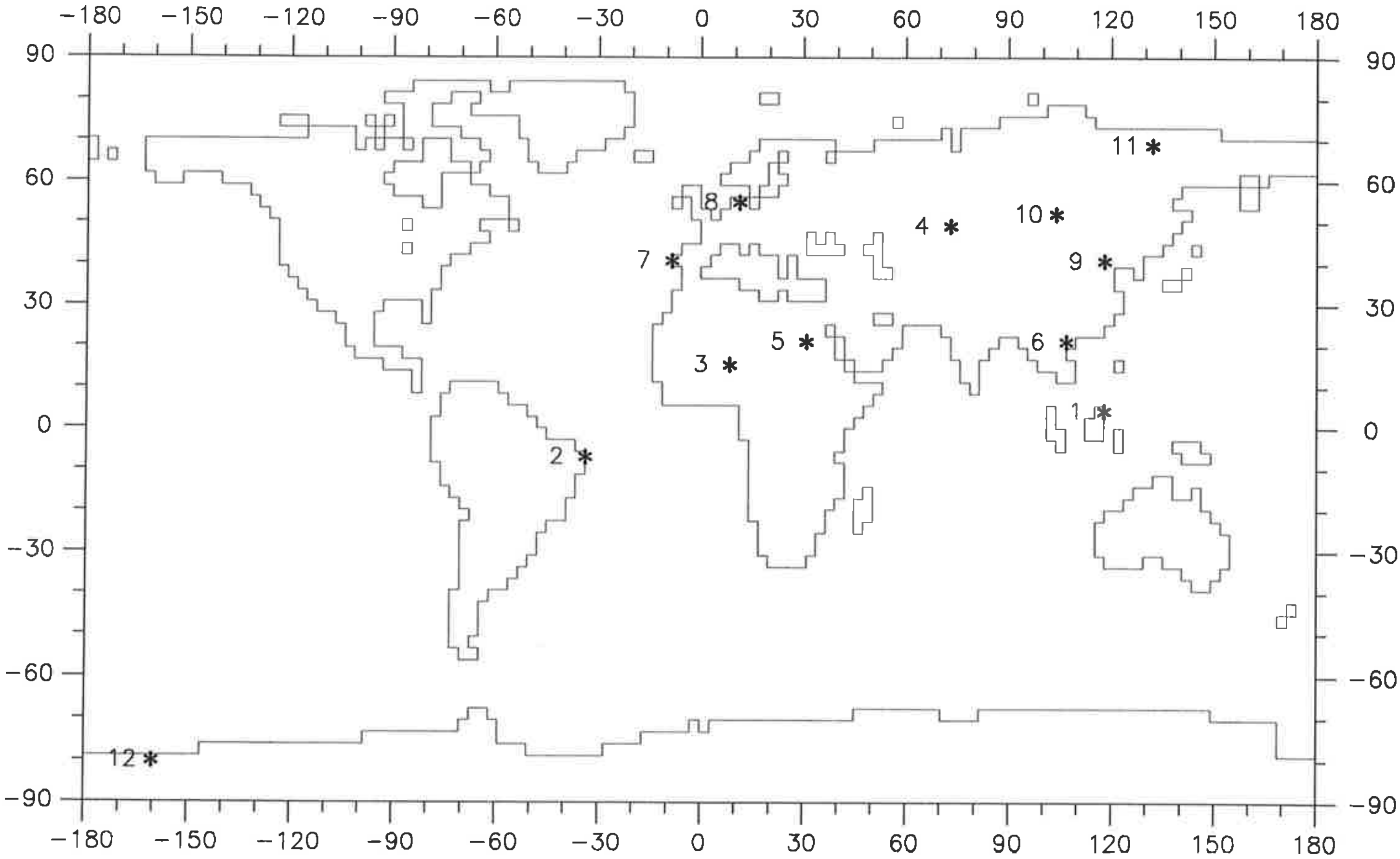

Figure 7: Geographical positions of the selected "climate stations" in Figure 6.

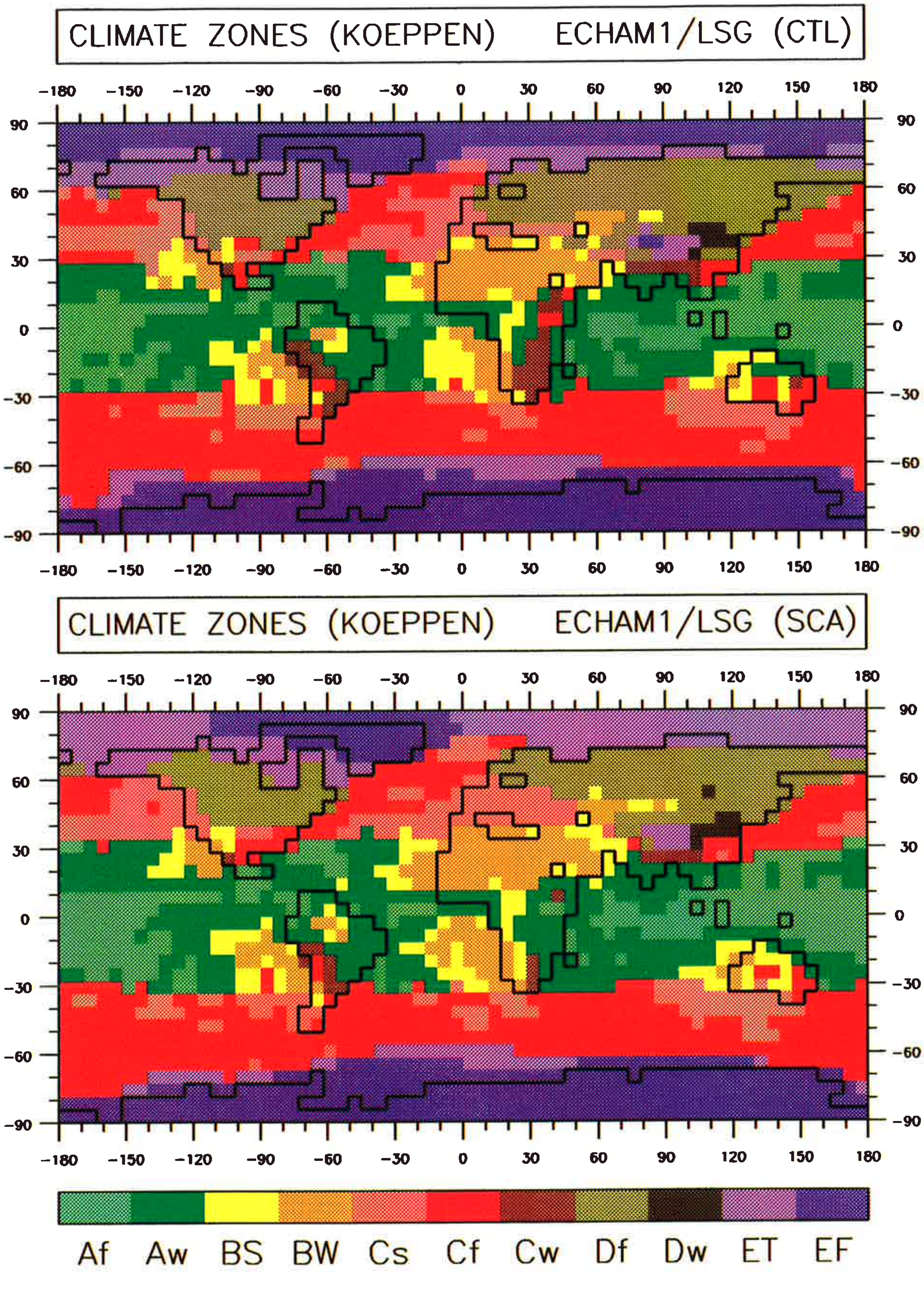

Figure 8: Köppen climate zones as simulated by the coupled model ECHAM1/LSG for the control simulation (upper panel) and for the Scenario A experiment (lower panel).

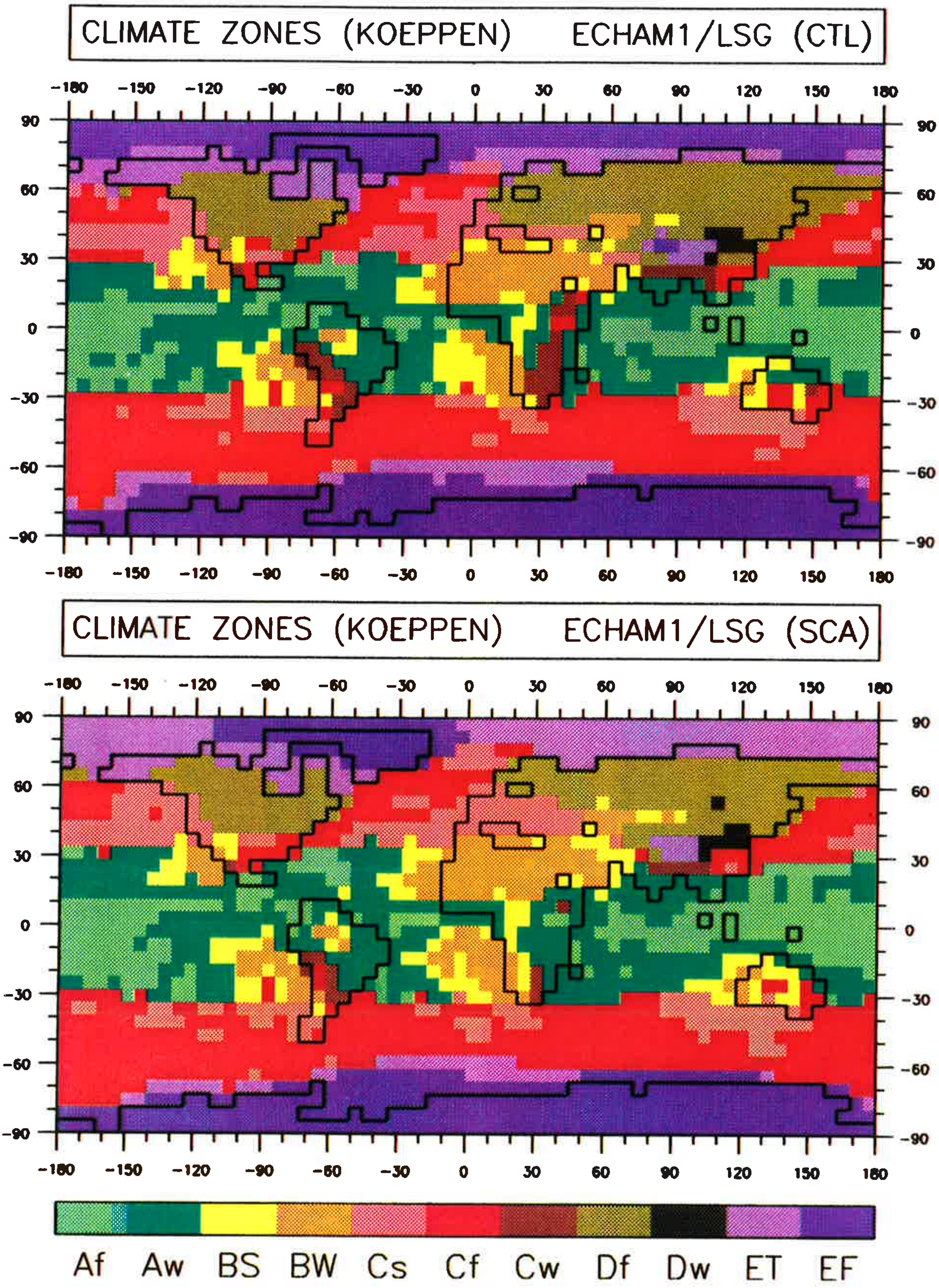

Figure 8: Köppen climate zones as simulated by the coupled model ECHAM1/LSG for the control simulation (upper panel) and for the Scenario A experiment (lower panel).

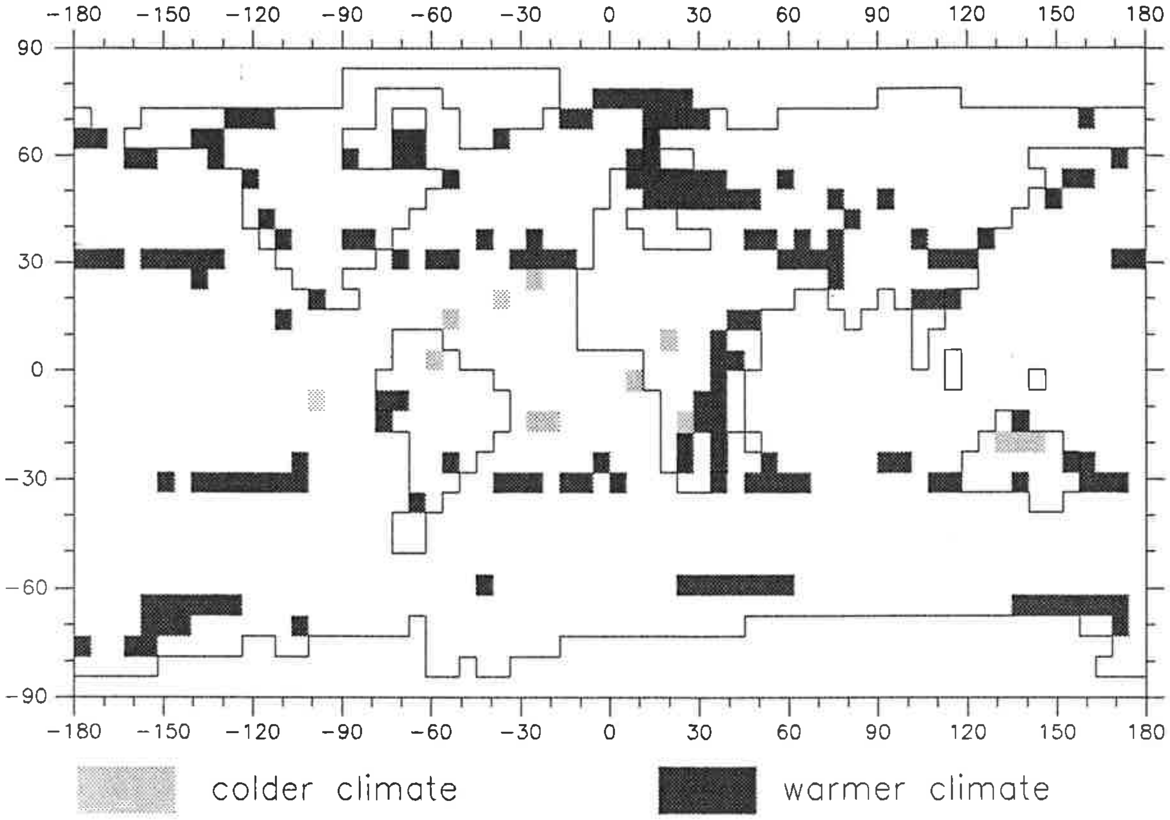

Figure 9: Change of climate types from Control (CTL) to Scenario A (SCA).

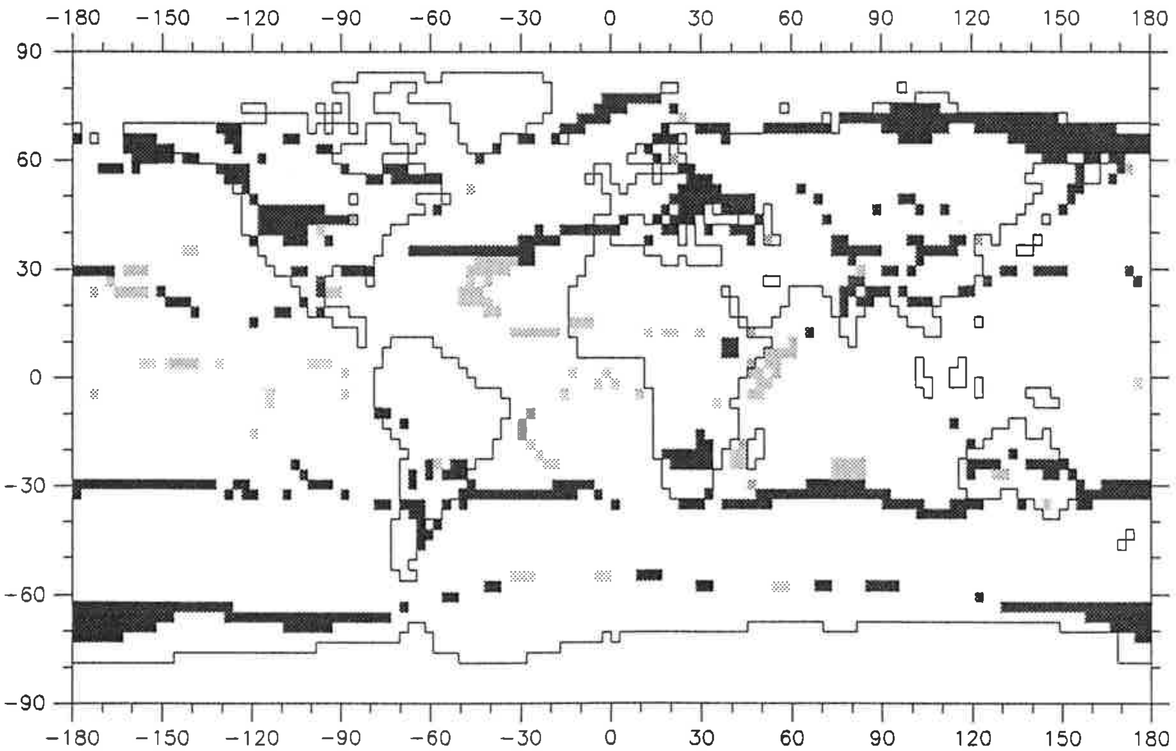

Figure 10: As Figure 9, but for the uncoupled T42 ECHAM3 simulations.